geosciences

MDPI

Article

Analysis of the Liquefaction Potential at the Base of the San Marcos Dam (Cayambe, Ecuador)—A Validation in the Use of the Horizontal-to-Vertical Spectral Ratio

Olegario Alonso-Pandavenes [1], Francisco Javier Torrijo [2,*] and Gabriela Torres [3]

[1] Faculty of Geology, Mining, Petroleum and Environmental Engineering-FIGEMPA, Universidad Central del Ecuador, Gilberto Gatto Sobral s/n, Quito 170521, Ecuador; omalonso@uce.edu.ec
[2] Department of Geotechnical Engineering, Research Centre for Architecture, Heritage and Management for Sustainable Development (PEGASO), Universitat Politècnica de València, Camino de Vera s/n, 46022 Valencia, Spain
[3] GEOTOP Ecuatorial Consulting, Quito 170507, Ecuador; geotop.equatorial@gmail.com
* Correspondence: fratorec@trr.upv.es

Abstract: Ground liquefaction potential analysis is a fundamental characterization in areas with continuous seismic activity, such as Ecuador. Geotechnical liquefaction studies are usually approached from dynamic penetration tests, which pose problems both in their correct execution and in their evaluation. Our research involves analyzing dynamic penetration tests and microtremor geophysical surveys (horizontal-to-vertical spectral ratio technique, HVSR) for analyzing the liquefaction potential at the base of the San Marcos dam, a reservoir located in Cayambe canton (Ecuador). Based on the investigations performed at the time of construction of the dam (drilling and geophysical refraction profiles) and the application of 20 microtremor observation stations via the HVSR technique, an analysis of the safety factor of liquefaction (SF_{liq}) was conducted using the 2001 Youd and Idriss formulation and the values of the standard penetration test (SPT) applied in granular materials (sands). In addition, the vulnerability index (K_g) proposed by Nakamura in 1989 was analyzed through the HVSR records related to the ground shear strain (*GSS*). The results obtained in the HVSR analysis indicate the presence of a zone of about 100 m length in the central part of the foot of the dam, whose *GSS* values identified a condition of susceptibility to liquefaction. In the same area, the SPT essays analysis in the P-8A drill hole also shows a potential susceptibility to liquefaction in earthquake conditions greater than a moment magnitude (M_w) of 4.5. That seismic event could occur in the area, for example, with a new activity condition of the nearby Cayambe volcano or even from an earthquake from the vicinity of the fractured zone.

Keywords: liquefaction; HVSR; San Marcos dam; Cayambe volcano; K_g vulnerability index; ground shear strain (*GSS*)

Citation: Alonso-Pandavenes, O.; Torrijo, F.J.; Torres, G. Analysis of the Liquefaction Potential at the Base of the San Marcos Dam (Cayambe, Ecuador)—A Validation in the Use of the Horizontal-to-Vertical Spectral Ratio. *Geosciences* **2024**, *14*, 306. https://doi.org/10.3390/geosciences14110306

Academic Editors: Florin Pavel, Alexandru Aldea and Cristian Arion

Received: 1 October 2024
Revised: 8 November 2024
Accepted: 11 November 2024
Published: 13 November 2024

1. Introduction

The soil's behavior under dynamic conditions and its response to strong ground shaking are among the most essential focuses in seismic hazard investigation. In a granular layer of no cemented sediments, the liquefaction process transforms it into a liquid state with characteristics of a solid-state mass. This is possible because the pore-water pressure is increased under cycling stress or shaking [1,2].

The liquefaction processes in areas where the conditions of saturation and phreatic levels are close to the surface (including sequences of fine to medium granular materials like sands and silts) are one of the main causes of damage and collapse of buildings and infrastructures when dynamic stresses occur in the event of an earthquake [3]. However, some features can vary from one plate to another, such as grain size and distribution, geometry and dimension, density, fine contents, and/or limit constraints of the deposit or

layers. All of these involve anomalous propagation (including amplification) of the seismic waves at the land surface [4].

In Ecuador, where the seismic hazard is high in all of the territory, these saturated granular terrains, especially recent sediments, have a wide propensity to liquefy in the event of an earthquake event, as it happened on 16 April 2016, in the Pedernales-Muisne earthquake [5]. Thus, probability analysis of liquefaction susceptibility is a vital investigation when the vulnerability affects, for example, earthen dams, with damage and failure occurring to varying degrees in dams worldwide [6].

In the natural lagoon of San Marcos, Cayambe Canton (Pichincha Province of Ecuador), a loose materials dam has been built and put into operation as a water reservoir for irrigation and drinking water. In this area, various investigations have been carried out, both for the construction and about natural hazards, by the owner of the infrastructure, the Decentralized Autonomous Government of the Province of Pichincha (from now on referred to as GADPP, the Spanish abbreviation of the Institution) [7]. In 2018, Torres [8] studied and defined the hazards related to volcanism and seismicity for said dam, evidencing the acceleration of the terrain on which the dam is founded and the possible effects of an eruption of the nearby Cayambe volcano. Subsequently, Alonso-Pandavenes et al. [9] carried out investigations on the axis and foot of the dam in order to determine and define the position and geometry of the rock basement using passive seismic techniques through the use of the horizontal-to-vertical spectral ratio (HVSR) and its correlation with the previous drilling performed for investigation of the area [10].

The research developed by Torres [8] preliminarily assessed the possible liquefaction potential based on field standard penetration tests (SPTs) performed in the exploration boreholes carried out for the construction of the infrastructure (personal communication; the corresponding report is not available). However, in the central area of the dam and the valley of the Azuela River, where it is located, these drilling and tests did not reach the rock basement (which is located at a greater depth than the 80 m explored) and SPTs could only be applied up to a 30 m depth. From this level, pyroclastic-type materials with a sandy matrix and the presence of thick boulders have appeared and prevented the execution of these types of geotechnical tests [7].

The present investigation will allow us to analyze, based on the results of the fundamental frequency of ground vibration (f_o) and its associated amplification (A_o), the potential or susceptibility of liquefaction of the ground at the base and surrounding areas of the San Marcos dam. We also intend to define areas around the dam with a propensity and possibility of liquefaction conditions arising under earthquake events. This analysis will be carried out using the so-called K_g vulnerability index [11] and its relationship with ground shear strain (GSS), also defined by Nakamura in 1997 [12]. Thus, it can demonstrate the efficacy, cost, and time economy of a simple survey in showing the sites beneath liquefaction that will be produced and the maximum intensity that can occur. In the most vulnerable areas, an assessment of said liquefaction capacity will be carried out to demonstrate and corroborate the data obtained through seismic tests and analysis based on the impact data from the SPT tests of the existing drillings and their potential to suffer this type of phenomenon.

2. Geographical Setting and Geological Framework

The area under investigation is located north–northeast of the Cayambe volcano, between the Pichincha and Napo provinces (Ecuador). This is a mountainous area close to the head of a glacial origin valley (circus) called the Azuela River, the most important watercourse in the area. The surficial deposits of the valley are dominated by fluvioglacial, volcanic, and volcaniclastic origin sediments that come from recent eruptions of the nearby volcano located less than 10 km from the study area (Figure 1, Cayambe volcano is out of the image to the southwest and is not shown in this detailed cartography) [8].

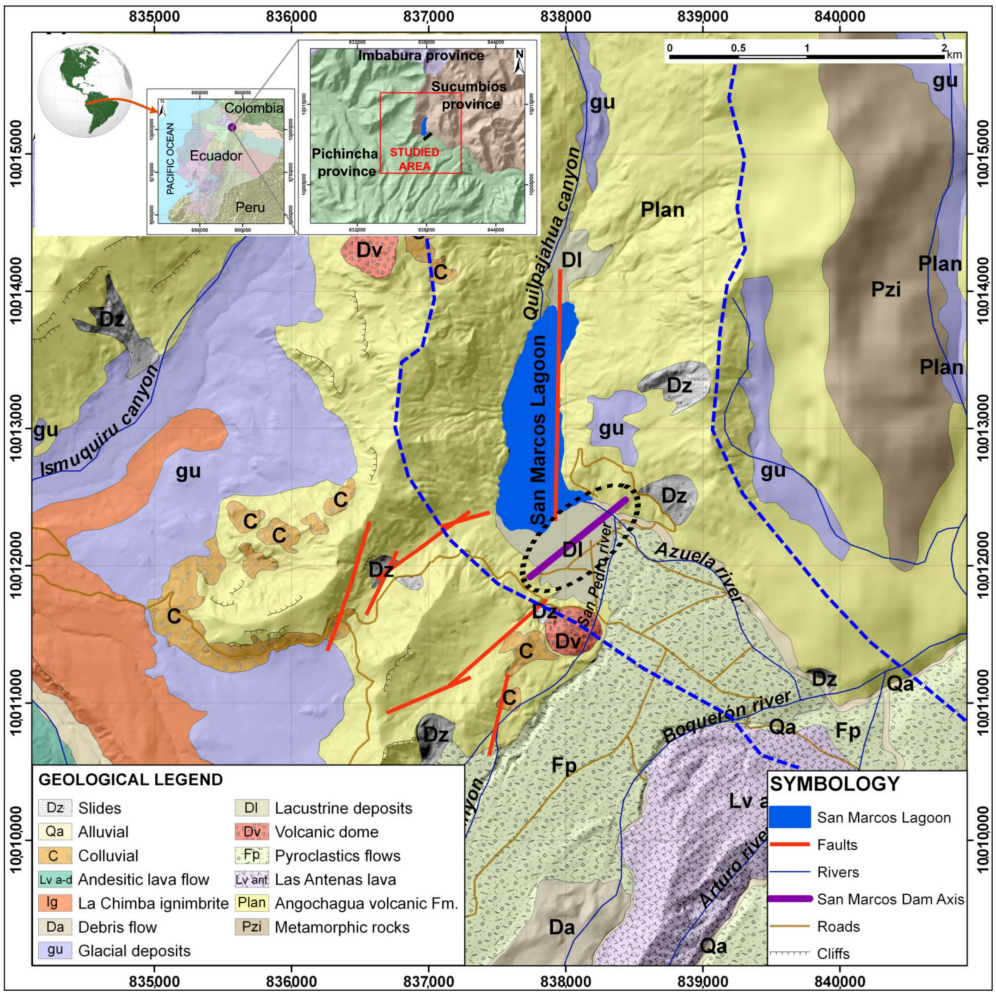

Figure 1. Situation and geology of the study area (black dotted oval at the center). A purple line marks the location of the axis of the dam, and the San Marcos valley feature is marked with a dashed blue line (modified from [8,9]).

For the hydraulic use of the existing natural lagoon (called Laguna de San Marcos), an earth dam with a height of 17 m high from the natural terrain and a length of 738 m at the crest was built [7].

The local geology of the dam area is dominated by the presence of a Pleistocene rocky basement, delineated by Alonso-Pandavenes et al. [9], and is composed of lavas and compact and cemented volcanic products (lavas, breccias, and tuffs) belonging to the Angochagua Formation (Figure 1). Several stratigraphic sequences of younger sediments have been deposited on top of these materials, referred to as the Cayambe Volcanic Formation. This formation originated in the nearby volcano and reached its most significant expression during the "San Marcos-type" eruption that occurred in the area about 4000 years ago. This eruptive event led to the deposition of pyroclastic material at the bottom that closed the valley and naturally dammed the water, starting the creation of the current San Marcos Lagoon [8,13].

Subsequently, and more recently, transported sediments were deposited in solid (glacial) or aqueous (alluvial and lacustrine) phases, which have shaped the current morphology of this area. These materials form a stratigraphic sequence in the area of the dam construction with a column of more than 35 m (in the central area, it exceeds 40 m), with predominant alluvial and intercalated lacustrine sediments (distal flow or low intensity) overlaying the pyroclastic material of the Cayambe Volcanics Formation [8,9] (see the cross-section in Figure 2).

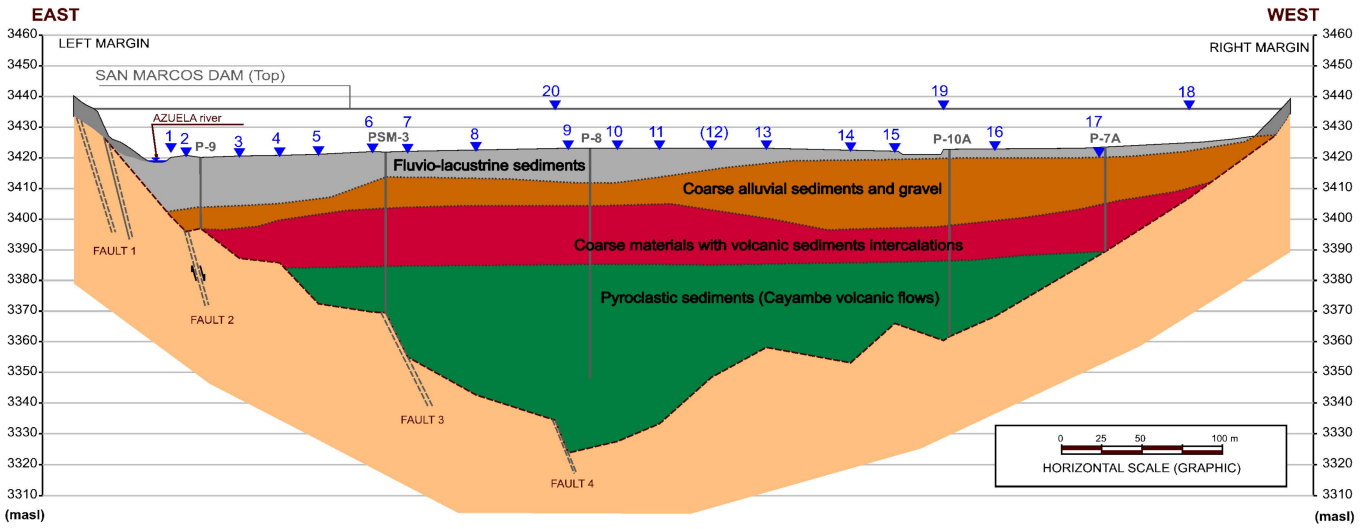

Figure 2. Geological cross-section of the San Marcos valley under the dam with an indication of the research points (blue inverted triangles), the boreholes (continuous grey vertical line), and the materials and structures defined in the studies prior to the construction of the dam. From top to bottom: Fluvio-lacustrine sediments, coarse sediments and gravels of alluvial origin, coarse sediments and intercalations of volcanic materials, and pyroclastic sediments from Cayambe volcano flows. The basaltic basement belongs to the Angochagua Formation, and colluvial sediments are also represented on both sides of the slopes at the margins. The cross-section corresponds to the purple line shown in Figure 1 (modified from [9]).

Regarding the tectonic structure of the dam construction area, the definition of faults and folds has not been wholly determined in previous studies due to the presence of thick and recent covering materials that mask these features. Some of these structural elements have been mapped and determined by Torres [8] and completed and defined in the Alonso-Pandavenes et al. [9] research.

The direction of these major structures identified in these studies is consistent with the deformation processes generated by the subduction zone of the western coast of Ecuador, where the Nazca plate subducts the South American plate [14]. This tectonic activity, together with nearby volcanic activity (for example, the Cayambe volcano resumed its activity for a few months in the period from 2016 to 2017) are the main focus of seismicity and earthquakes in the area [8,14,15].

The area and surroundings of the San Marcos dam are located in a high seismic risk zone, according to the definition and assessment included in the Ecuadorian Seismic Classification within the NEC-SE-DS Ecuadorian Earthquake Resistant Standard [16], the general value of rock acceleration (peak ground acceleration, PGA) admitted and calculated by said standard for the study area being of the order of 300 Gal.

However, according to the Torres [8] investigations through probabilistic and deterministic seismic hazard analysis (PSHA and DSHA), it has been confirmed that these seismic demand acceleration values for the foundation area of the San Marcos dam could reach 400 to 500 Gal due, above all, to the local effect that is also called site effect (amplification factors due to the presence of a thick sedimentary cover of low to medium compaction).

3. Methodology and Previous Knowledge

In 2009, the GADPP [7] began designing and constructing a loose materials (earth) dam on the southern side of the San Marcos lagoon. This infrastructure, intended for damming water for irrigation and human consumption, is founded over the most superficial sediments of the fluvial-lacustrine type (see Figure 2) on a flat artificial terrain improvement without constructing a lower curtain. The axis of the dike has a length of more than 700 m,

with a southwest–northeast direction, and a height of 17 m above the area's natural terrain (see location in Figure 1).

Due to the morphological configuration of the valley where the dam is located (Azuela Valley), limited by compact rocky materials on both sides and pyroclastic materials in the bottom and towards the southeastern area, it can be considered that the area where the San Marcos dam is located has suitable undrained conditions for the materials that constitute its foundation and support.

In dynamic soil stresses, for example, those produced during an earthquake, cyclic loads occur that infer volume changes (decrease) in granular materials due to the reorganization of their particles. When the affected materials are saturated in undrained conditions, these loads are transmitted directly to the water, increasing pore pressure, which decreases the shear stress of the materials and their behavior like a liquid. This is known as the liquefaction phenomenon [17].

Therefore, this soil behavior under dynamic stress will influence the stability and integrity of a structure or construction built on materials that can liquefy (soil–structure interaction), as is the case of the San Marcos dam. According to the data collected in the performed drilling for its design and construction, the most superficial part of the materials where the structure is founded has the main characteristics to exhibit liquefiable behavior. These materials are of a fine granular type (sands and silts that are not too compact) with a water table throughout the area at or close to the surface (less than 2.0 m depth, established in the surveys [7]).

Based on laboratory tests and earthquake data, Ishihara's research [18,19] made it possible to relate the deformation between the shear stress and the dynamic properties of the terrain. These studies were the starting point for Nakamura [12] to define his vulnerability index (K_g) established from environmental vibration measurements through the following formula:

$$K_g = e \frac{\left(\frac{A_0^2}{f_0}\right)}{\pi^2 V_b} \quad (1)$$

where e is the effectiveness, f_o is the value of the fundamental frequency of ground vibration, A_o is its associated amplification or the H/V spectral ratio value (last both obtained from the results of the processing of the HVSR tests and the analysis of the dispersion or ellipticity curve), and V_b is the rocky basement shear-wave velocity [12].

Considering a value of e = 60% and a shear velocity = 600 m/s (Nakamura 1997 identifies this with the lower limit for the rock or basement), and a constant value for all places (10^{-6}), this index would be defined in a simplified way, from Equation (2):

$$K_g \sim \frac{A_0^2}{f_0} 10^{-6} \quad (2)$$

In this simplified form, the K_g value is used in most publications where the authors consider its results, and the simplification is valid, even for Nakamura [12,20–24].

From this index (defined as "vulnerability", although it is not that term directly), it is possible to estimate the shear stress of the surface materials, which can be related to the potential impact that a dynamic stress (as an earthquake) can produce on the column of sedimented soil overlaying a basement (considering the area like a two-layer model). This K_g index can then be applied in the study of soil liquefaction or the potential initiation of a landslide, in the relationship established by Nakamura [12] between the K_g vulnerability index and the shear stress or deformation or ground shear strength (GSS) according to the following equation:

$$GSS\ (\gamma) = K_g\ 10^{-6}\ \alpha \quad (3)$$

where α would be the acceleration to which the ground is subjected in the event of an earthquake (expressed in Gal). Table 1 shows a distribution where the size of the deformation (GSS) and the dynamic properties of the terrain are related, along with the phenomena that

can develop due to said deformation. As observed, strain values greater than 10^{-2} can produce landslides on soil slopes, compaction (in drained conditions), or liquefaction (in undrained conditions) and, thereby, contribute to collapse or damage to the soil interaction with an infrastructure [19].

Table 1. Relationships between deformation (GSS) and dynamic soil properties. Modified from Nakamura [12] and based on the publications of Ishihara [18,19].

Size of *GSS* (γ)	10^{-6}	10^{-5}	10^{-4}	10^{-3}	10^{-2}	10^{-1}
Phenomena	Wave, Vibration		Crack, Settlement		Landslide, Soil compaction *Liquefaction*	
Dynamic Properties	Elasticity		Elasto-plasticity		Collapse	
			Repetition effect, Velocity load effect			

In the present investigation, the calculation technique that will be used is based on HVSR test measurements in the area of the bottom and crest of the San Marcos dam in order to assess the liquefaction potential. To do this, once the field data have been obtained and the ellipticity curves have been processed and analyzed, the value of the size of the deformation can be obtained by defining in the areas where a *GSS* value (γ) is greater than 10^{-2}, using Equation (3). These will have the capacity or potential for liquefaction phenomena during a seismic event [18,19]. This does not mean these liquefaction phenomena will occur, even under the conditions considered in this study, since there may be variables in other factors and parameters not analyzed in the research. However, it is an assessment to remember in the future of the monitoring processes during dam exploitation and, above all, when a major seismic event occurs.

On the other hand, studies on the liquefaction processes of granular materials under dynamic conditions were published by Youd and Idriss [2]. These authors define the safety factor against liquefaction (SF_{liq}) as a relationship between the acting forces, the cyclic stress ratio (*CSR*), and its resistance to presenting said phenomenon, the cyclic resistance ratio (*CRR*):

$$SF_{liq} = \frac{CRR}{CSR} \quad (4)$$

One of the most common ways to analyze liquefaction is through the execution of SPTs (standard penetration tests) during borehole drilling, as recommended by the National Center for Earthquake Engineering Research, summarized in [2].

This type of test is one of the most used in geotechnical research. However, it must be used with great care in analyses related to liquefaction processes due to the execution procedures (with many human errors) and lack of repeatability in many cases [25]. These analyses using SPTs are based on the considerations made by Seed and Idriss [26] and Seed et al. [27]. They established a correlation between liquefaction and the ground characteristics through the tapping obtained in said test (N_{SPT}). This criterion relates the average cyclic stresses, that is, the seismic demand for a design earthquake, with the number of blows of the SPT corrected and normalized for an overload of 100 kPa, called $(N_1)_{60}$. This methodology has been obtained experimentally from historical case studies [2].

The *CRR* rating curves, the resistance of the soil that opposes liquefaction, were developed for granular soils with different percentages of fines (5%, 15%, and <35%) in case of earthquakes whose moment magnitude (M_w) is of 7.5, which would be the one considered in Equation (3). A correction factor adapted to the magnitude considered must be applied for earthquake magnitude conditions different from the previous formulation, as in Equation (3). Youd and Idriss [2] published and endorsed these relationships based on proposals from previous research by Idriss himself. As expected, when the calculated safety factor SF_{liq} value is less than unity, the terrain will present or have the capacity or susceptibility to liquefy.

The HVSR passive seismic technique uses the microtremor or natural vibration of ground measurements to evaluate the susceptibility of a sedimentary layer (mostly soils) to liquefy, according to Nakamura [12,28] (expressions shown in Equations (1) and (2)). Thus, some authors use the K_g index to define the liquefaction potential of soil deposited over a basement when it is over 10 [21,29–32]. Thus, using those values, the *GSS* value is estimated from Equation (3) for assessing the likelihood of large-scale deformation relating to liquefaction for values over 10^{-2} [33]. HVSR seismic measures have some advantages such as their rapidity, low cost, and repeatability, but, on the other hand, no samples can be obtained, thin layers can be invisible, and most importantly, it analyzes small stresses while earthquakes create high stress in the soils [34].

The geophysical research campaign consisted of the application of the HVSR technique carried out on a total of 20 single station points, which were distributed along the base of the dam, its crest, and a parallel alignment separated by about 50 at 150 m, as can be seen in Figure 3. Three tests, numbered 18, 19, and 20, were carried out on the dam's crest, while points 1, 12, 14, and 17 were measured in an area further away from the foot of the dam; their results were used due to the continuity in the materials that make up the area.

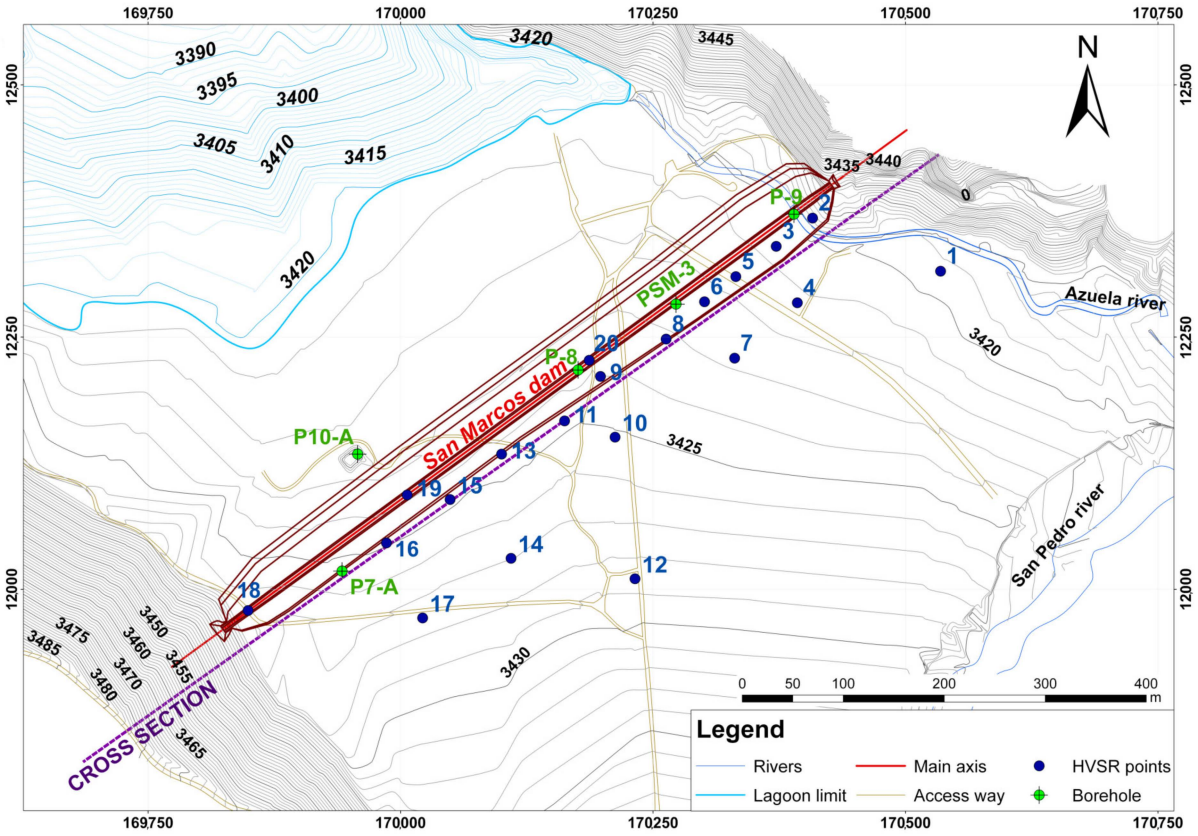

Figure 3. Map showing the location of the HVSR research points in the San Marcos dam area (blue dots) and boreholes (in green circles). The geological cross-section position through the Azuela Valley, shown in Figure 2, is also indicated (modified from [9]).

The equipment for measuring environmental noise or microtremors was set up at each point. This equipment consists of three geophones (triaxial configuration) with a 2.0 Hz natural frequency. The geophones are arranged according to the three directions of space: N–S, E–W, and vertical Z (Figure 4a). The measurement unit is connected to a computer that controls the measurement parameters (recording time and measurement frequency) and stores the data (Figure 4a and a view of the bottom of the dam measuring a station point, Figure 4b).

(**a**) (**b**)

Figure 4. Detailed view of the measurement equipment installed on the ground recording the #4 HVSR station (**a**). The #8 research point with the equipment measuring and the view of the dam's downstream side in the image's background (**b**).

The records measured at each HVSR station point were obtained by meticulously capturing the surrounding vibrations for 20 min. This thorough data collection process ensures the reliability of our findings [35].

4. Results

The HVSR technique surveys were processed using the free software program GEOPSY (www.geopsy.org [35,36], accessed on 21 October 2023, 3.5.1 release), which consists of analyzing and separating the time windows of the records from the three components obtained in the field (Figure 5a). The invalid or poor-quality data in the windowing separation were then erased, and a fast Fourier transform was applied to the valid data to obtain the frequency distribution curve (Figure 5b). From these results, the dispersion curve, also called ellipticity, was obtained, and relates the spectral ratio (H/V) of the horizontal component to the vertical one, or amplification (A_o), with the frequency distribution. Thus, for each point tested, a pair of values is obtained, which relates the maximum amplification A_o with the frequency considered fundamental to the terrain in the area (f_o) that defines the conditions of Nakamura's two-layer model [35].

Once the field data of the 20 points tested in the surroundings of the San Marcos dam were processed (see Figure 3), a pair of values was obtained for each, where the range of the natural frequency of the terrain was between 0.12 Hz and 61.26 Hz, while the value of the amplification A_o was between 0.95 and 9.33, this being dimensionless (see three first columns in Table 2).

Table 2 also shows the results obtained for each of these 20 HVSR measurement tests carried out and, consequently, the calculated value of the vulnerability index K_g (dimensionless) according to Equation (2) and the calculated value of the *GSS* (γ) according to Equation (3), shown in the fourth and fifth columns. In the study area, the values obtained in the research carried out by Torres [8] for the area surrounding the location of the San Marcos dam were 501 Gal for a return period of 500 years, a value that was used in the application of Equation (3). This value includes the PGA acceleration in rock and the potential amplification produced by the thick sedimentary terrain that can happen in the dam's construction area. Following the abovementioned criteria, six measurement points were identified where the value obtained from the *GSS* parameter is greater than 10^{-2}, i.e., they have susceptibility to liquefy. These points correspond to the HVSR single station tests 8, 9, 10, 13, 14, and 20, and they are indicated as YES (*GSS* capacity or susceptibility valorization) in the sixth column of Table 2. At the 11 and 15 station points, the obtained values are at the limit of susceptibility (included as YES too), which is why they were considered in this list with said exception (acceptance between parentheses).

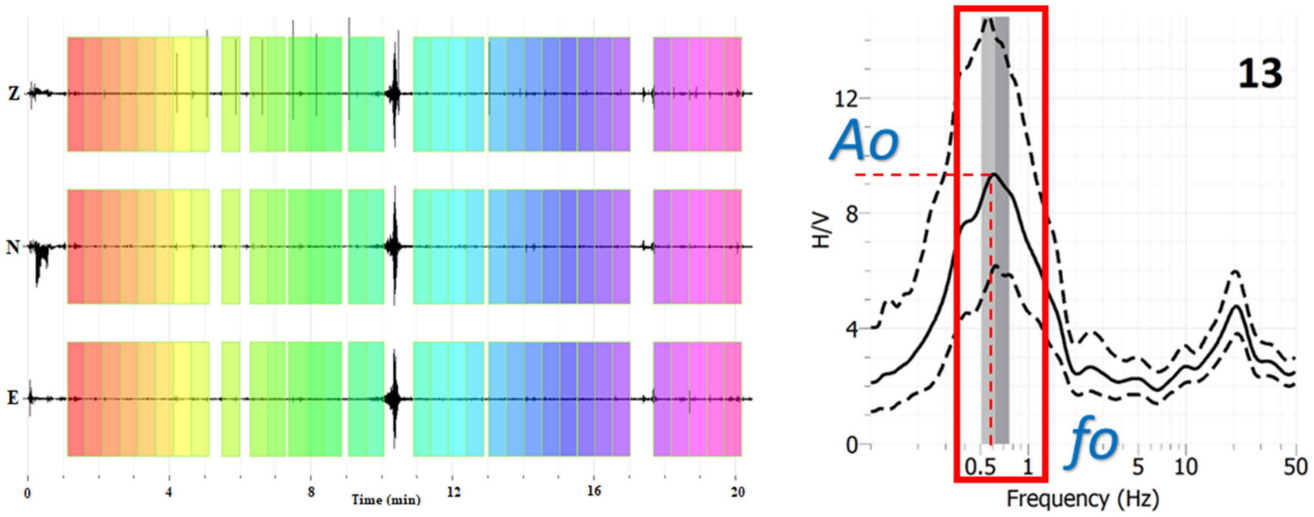

(**a**) (**b**)

Figure 5. (**a**) The field record of point #13 includes the definition of 20 s time windows (in color) over the three components (N–S, E–W, and Z, from top to bottom) for subsequent processing. (**b**) The ellipticity curve obtained for point #13 is shown, where the values of f_o and A_o are indicated (the red rectangle highlights the main peak of the curve).

Table 2. Results of processing the HVSR measurements at the San Marcos dam area and calculating K_g and *GSS* with analysis of the susceptibility from those values. See the explanation in the text.

HVSR Points	f_o (Hz)	A_o	K_g	*GSS* (γ)	SUSCEPT. *GSS*	SUSCEPT. by K_g
1	61.26	1.90	0.1	1.92×10^{-5}	NO	NO
2	33.05	3.45	0.4	1.17×10^{-4}	NO	NO
3	10.01	4.94	2.4	7.92×10^{-4}	NO	NO
4	7.36	0.95	0.1	3.99×10^{-5}	NO	NO
5	1.51	4.92	16.0	5.21×10^{-3}	NO	YES
6	1.61	3.70	8.5	2.76×10^{-3}	NO	(YES) [1]
7	0.18	1.45	11.7	3.80×10^{-3}	NO	YES
8	0.29	3.36	38.9	1.27×10^{-2}	YES	YES
9	0.12	3.10	80.1	2.60×10^{-2}	YES	YES
10	0.14	3.31	78.3	2.54×10^{-2}	YES	YES
11	0.18	2.14	25.4	8.27×10^{-3}	(YES) [1]	YES
12	0.38	2.81	20.8	6.75×10^{-3}	NO	YES
13	0.67	8.74	114.0	3.71×10^{-2}	YES	YES
14	0.27	9.33	322.4	1.05×10^{-1}	YES	YES
15	1.21	5.35	23.7	7.69×10^{-3}	(YES) [1]	YES
16	1.36	5.17	19.7	6.39×10^{-3}	NO	YES
17	12.58	4.49	1.6	5.21×10^{-4}	NO	NO
18	17.11	7.42	3.2	1.05×10^{-3}	NO	NO
19	0.36	2.37	15.6	5.07×10^{-3}	NO	YES
20	0.19	3.61	68.6	2.23×10^{-2}	YES	YES

[1] Conditional acceptance (see explanation in the text).

The last column of Table 2 indicates the analysis using only K_g, using Equation (3), as an evaluation of susceptibility to liquefy (used by some authors). In this situation, the susceptibility was classified according to whether it exceeded or was less than this limit of 10, considering point number 6 as susceptible because its value is close to 10 and the location is between HVSR stations 5 and 8, which are susceptible [12].

Additionally, the K_g index is visually represented in Figure 6, where a new analysis of the values obtained by the HVSR tests was conducted, using Equation (2) to establish the

liquefaction potential zone. The K_g index, depicted as a bar, represents the most probable accelerations observed in the study area during an earthquake. According to Torres [8], the PGA of the area is established between 275 Gal (minimum obtained for rock also in the NEC-SE-DS [16] and 550 Gal as the maximum value of acceleration expected in the area, considering the amplification of the site effect. The graph also displays the V_s velocities for sediments in the area (ranging from a minimum of 120 m/s to a maximum of 250 m/s), with the average value of 190 m/s represented by a dashed line (see Figure 6). These V_{s30} values were obtained by calculating the V_s from the SPTs in the different boreholes where there was available information, according to the formulation for all types of soils and sands shown in Sil and Haloi [37]. A V_{s30} average of 185 m/s was obtained with extremes of 135 m/s and 215 m/s.

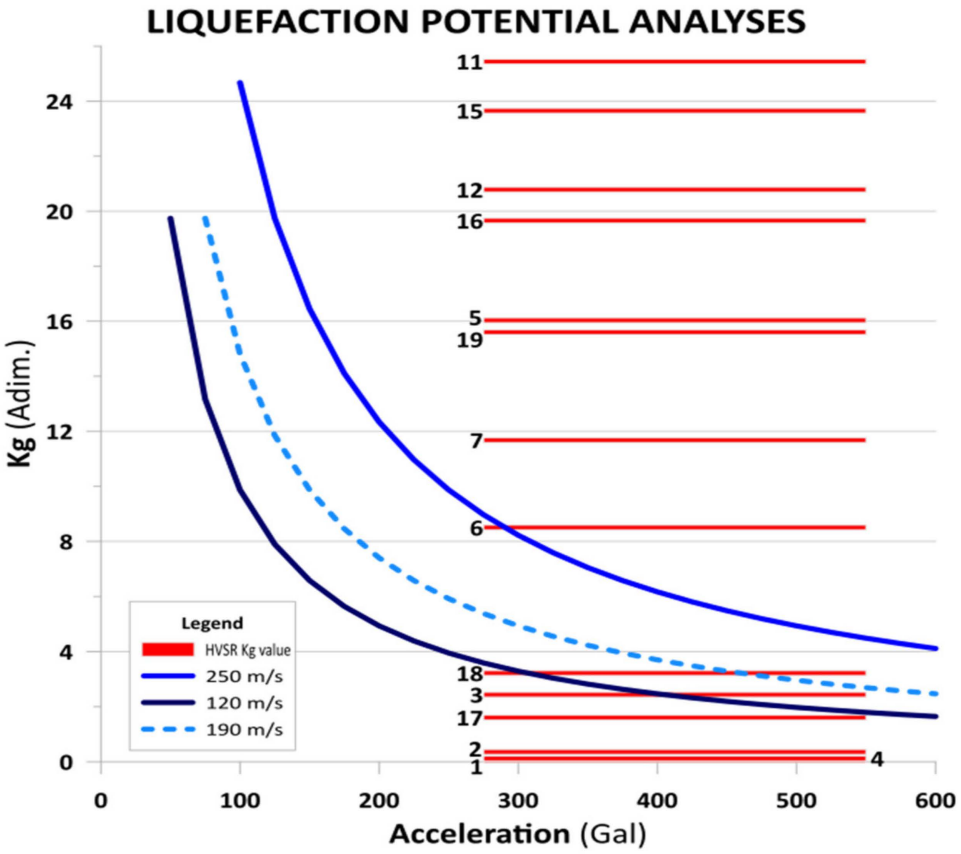

Figure 6. Analysis of the liquefaction potential for the HVSR tests carried out in the area based on the K_g value obtained (horizontal red lines), according to Table 2. For greater clarity of the graph, only values up to 26 are represented on the ordinate axis (K_g); tests that presented higher values are not represented since they exceed the V_s value curve of 250 m/s for the acceleration intervals 275 Gal to 550 Gal indicated.

In this graph, the points above or at the limit associated with a V_s would be or present susceptibility to liquefaction, while those below them are considered stable. Also, it was considered in Figure 6 that the points whose calculated K_g value is greater than 26 be excluded for better-detailed representation (i.e., points 8, 9, 10, 13, 14, and 20) and since they are clearly above the V_s value of 250 m/ s. The HVSR points 5, 7, 11, 12, 15, 16, and 19 are located above any V_s value, which indicates their high susceptibility to suffering liquefaction processes for the accelerations considered and for a value of V_s average between the indicated ranges.

HVSR points 3, 18, and 6 present values of the K_g index located between the V_s limit lines (120 m/s and 250 m/s) for the expected accelerations in the study area. Points 3 and 18 are located at the ends of the dam (see Figure 3) and would present susceptibility in

cases of accelerations over 475 Gal and 300 Gal, respectively (for V_s values over 120 m/s). In the case of the HVSR point 6, it would be susceptible to liquefying for accelerations under 285 Gal at V_s values of 250 m/s. On the other hand, points 1, 2, 3, 4, and 17 are clearly below any V_s curve value considered, so they would be in stable zones (see Figure 6 and Table 2 for references).

Both susceptibilities (from Table 2) were combined with the above results obtained and analyzed. It was observed that points 8, 9, 10, 11, 13, 14, and 20 coincide in both analyses, which indicates a high liquefaction potential for those areas. Points 3, 5, 6, and 18 could be ruled out if liquefaction occurred (given by some small *GSS* values), and the same for points 15, 16, and 19.

Figure 7 presents a representation map and identification of the susceptible-to-liquefaction points indicated above through a red circle. The points are around or adjacent to the position of the P-8A borehole, located in the central area of the dam. This survey shows where the greatest thickness of superficial granular sediments, related to finer fills, could correspond to investigated drainage paleochannels of the ancient San Marcos lagoon. PSM-3 borehole reached SPT refusal, too shallow (less than 7 m) to be helpful in this investigation [9].

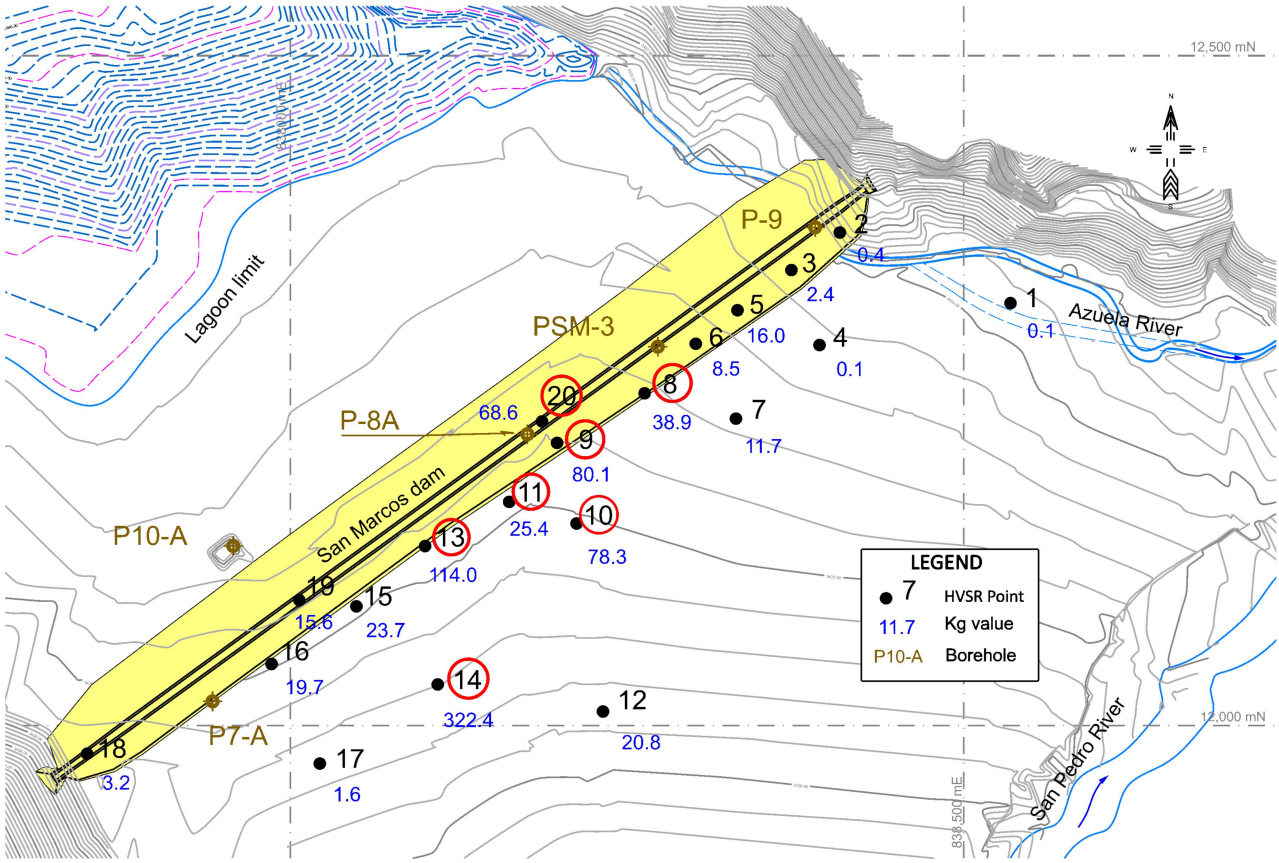

Figure 7. A map of K_g parameter distribution values (referenced in blue). The HVSR station points in the image are identified with a red circle where liquefaction susceptibility has been evident depending on the *GSS* value. They correspond to those susceptible to liquefaction whose values exceed $\Upsilon \geq 10^{-2}$ (modified from [9]).

Thus, the P-8A borehole was used as the reference in the analysis to compare the results of the liquefaction factor SF_{liq} through the analysis of SPTs with those obtained in this geophysical processing.

Table 3 presents a summary of the logging of the P-8A survey based on the SUCS soil classification tests (obtained from the samples extracted in the SPTs). The impact values are not available below a depth of 30.0 m (it was assumed that rejection was obtained in the

impact when pyroclastic materials from the Cayambe Volcanic Fm. are found; see Figure 2). Drilling began at meter 1.5 because the upper meter comprises peat-type materials and paramo lacustrine sediments with zero resistance to the dynamic penetration test.

Table 3. Liquefaction analysis for drilling P-8A (Youd and Idriss, 2001 procedure). Values for the case of an average site acceleration of 0.331*g* and a maximum earthquake moment M_w of 5.0.

S.U.C.S.-Type Materials	Depth (m)	N $_{SPT}$ (blows)	$(N_1)_{60\,CS}$	CRR corr.	CSR	Safety Factor SF_{liq}	Condition [1]
SM	1.5	2	2.531	0.206	0.263	0.783	(C)
SM	2	3	3.694	0.232	0.311	0.746	(C)
SM	3	5	6.300	0.279	0.333	0.838	(C)
SP-SM	4	6	7.662	0.298	0.323	0.923	(C)
SP-SM	5	7	8.852	0.314	0.302	1.040	(C)
SP-SM	6	6	7.420	0.263	0.278	0.946	(C)
SP-SM	7	9	10.808	0.339	0.251	1.351	(D)
SP-SM	8	13	15.548	0.454	0.226	2.009	(D)
SP-SM	9	12	13.588	0.386	0.204	1.892	(D)
SP-SM	10	16	17.916	0.490	0.185	2.649	(D)
SP-SM	11	15	15.911	0.421	0.170	2.476	(D)
SM	12	9	8.872	0.251	0.159	1.579	(C)
SP-SM	13	13	12.523	0.324	0.151	2.146	(D)
SP-SM	14	9	8.283	0.231	0.144	1.604	(C)
SP-SM	15	13	11.631	0.293	0.140	2.093	(C)
SP-SM	16	11	9.475	0.246	0.136	1.809	(C)
SP-SM	17	12	10.007	0.253	0.134	1.888	(C)
SP-SM	18	11	8.890	0.228	0.132	1.727	(C)
SP-SM	19	15	11.810	0.279	0.131	2.130	(C)
SP-SM	20	17	13.080	0.299	0.127	2.354	(D)
SP-SM	21	14	10.286	0.244	0.125	1.952	(C)
SP-SM	22	17	12.230	0.276	0.123	2.244	(C)
SM	23	20	14.165	0.308	0.121	2.545	(D)
SM	24	31	22.508	0.478	0.119	4.017	(D)
SM	25	20	13.287	0.285	0.116	2.457	(C)
SM	26	20	12.888	0.275	0.114	2.412	(C)
SM	27	25	16.021	0.326	0.112	2.911	(D)
SM	28	22	13.488	0.279	0.110	2.536	(C)
SM	29	19	11.161	0.239	0.108	2.213	(C)
SM	30	18	10.194	0.222	0.106	2.094	(C)

[1] Liquefaction conditions symbology: (C) = Contractive, (D) = Dilative. Notes: N $_{SPT}$: raw blows from the SPT; $(N_1)_{60\,CS}$: corrected blows from SPT; CRR corr.: the corrected cyclic resistance ratio value; CSR: the cyclic stress ratio values.

According to the bore hole logging, the superficial layers correspond to the SM SUCS-typology (sands), which would be fine sands with a pumice-granulated composition, according to the description of the soil nucleus [7]. This gives way to a 19.0 m section composed of poorly graded fine sands (SP-SM), which present intercalations of a section of SM fine sands at the 12.0 m depth. From 22.0 m onwards, the presence of silty areas with gravel is identified in the drilling (possibly related to the deposition of lahars or pyroclastic flows removed and reworked in the aqueous phase, exceeding values of 20 in N_{SPT} tests the aqueous phase from this depth onwards).

Regarding SPTs blowing up to 7.0 m, values lower than ten are detected, increasing this number of blows between 8.0 m and 22.0 m to an average value of around 13 (with extremes in the range of 11 to 17). Finally, note that in our survey, the water table detected was established at a depth of 2.0 m below the starting level (within the less compact and peaty type materials), which is a value considered to be very superficial.

Following the methodology indicated in Youd and Idriss [2] using Equation (4), the results of the calculated data for safety factors are shown in the fifth to seventh columns of Table 3. These calculations established an average site acceleration of 0.331*g* and a

maximum earthquake expected at the zone M_w = 5.0 (source-to-site epicenter distance of 38 km), according to probabilistic seismicity analyses (PSHA) performed by Torres [8] and indicated in the norms [16].

From these calculations, it can be seen that the tested materials present, from shallow to 6.0 m, a safety factor value lower than 1.0 with a contractive behavior (at 5.0 m the obtained value is close to 1.0 and it is included). Moreover, the SF_{liq} (seventh column of Table 3) for 6 m thickness is close to unity (0.85 on average). The last column of Table 3 indicates the characteristics of the materials in terms of their behavior (contractive or dilative). However, this determination would require complementary information for accuracy, such as the proportion of fines in the sample, which is not currently available.

The values shown in Table 3 consider some average conditions, such as those expressed in MIDUVI's (2015) norm and from PSHA analysis. However, Figure 8 shows that the M_w can be exceeded, even for Cayambe volcano earthquakes (produced at the "San Marcos-type" eruption scenario) with a probable M_w 6.3 earthquake 38 km epicenter location away from the San Marcos dam area. Also, it must be considered that the amplification due to the thick sediment stratigraphy in around the dam area can reach the ground acceleration to an extreme value of 0.51 g [8].

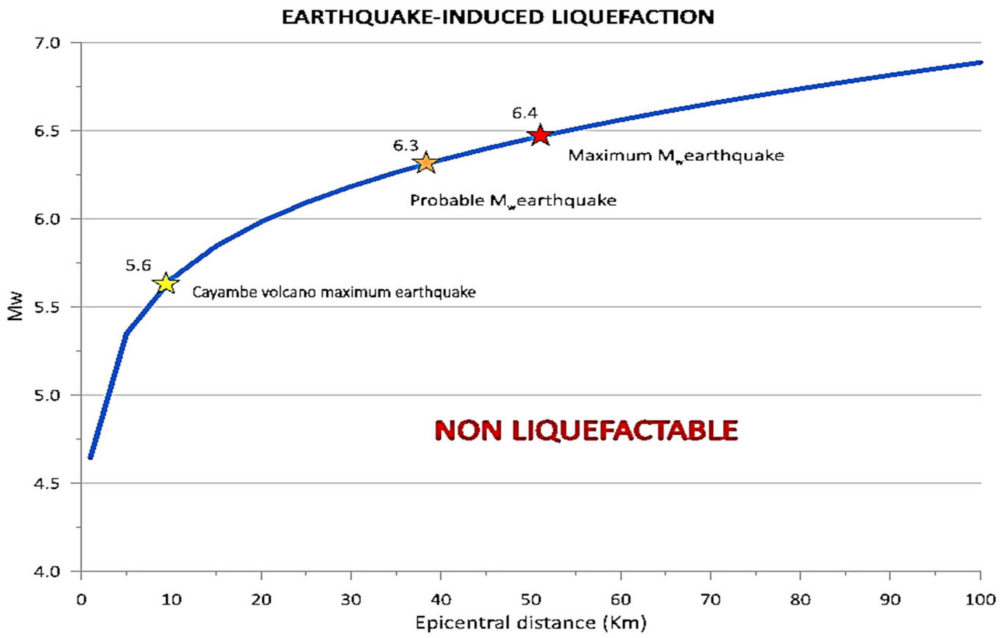

Figure 8. Earthquake-induced liquefaction representation from an epicentral distance at different M_w magnitudes, using the Ambraseys [38] relation in Equation (5). They are indicated for the distances from the Cayambe volcano (5.6 M_w maximum earthquake), the probable M_w earthquake (6.3 value, with epicenter 37 km away), and the maximum M_w earthquake (6.4 M_w) obtained from the Deterministic Seismic Hazard Analysis (DSHA) and Probabilistic Seismic Hazard Analysis (PSHA) seismic risk analysis performed by Torres [8].

Considering these maximum seismic risk values and for the same conditions and the same borehole (P-8A) located at the center of the dam and the valley where the maximum sediment thickness was developed (see Figure 2), we performed calculations for the variation of the liquefaction safety factor from different M_w earthquake scenarios, starting from the magnitude M_w 3.5 as the reference under which it is considered that liquefaction phenomena cannot be produced, through the M_w 6.0, a value that exceeds those M_w earthquakes from the nearest source, the Cayambe volcano (Table 4).

Table 4. Liquefaction analysis for drilling P-8A using the procedure of Youd and Idriss [2] (same as was shown in Table 3). Values for the case of an acceleration of 0.51*g* (550 Gal) and several M_w moments.

Depth (m)	Safety Factor SF_{liq} 1	Safety Factor SF_{liq} 2	Safety Factor SF_{liq} 3	Safety Factor SF_{liq} 4	Safety Factor SF_{liq} 5	Safety Factor SF_{liq} 6	Safety Factor SF_{liq} 7
Acc.: 550 Gal [1]	3.5 M_w	4.0 M_w	4.5 M_w	5.0 M_w	5.2 M_w	5.6 M_w	6.0 M_w
1.5	1.135	0.843	0.647	0.511	0.468	0.395	0.340
2	1.087	0.805	0.619	0.486	0.446	0.377	0.322
3	1.240	0.914	0.698	0.549	0.502	0.423	0.360
4	1.387	1.019	0.775	0.607	0.553	0.466	0.396
5	1.602	1.168	0.882	0.687	0.626	0.522	0.444
6	1.506	1.088	0.818	0.631	0.572	0.478	0.403
7	2.227	1.595	1.186	0.906	0.818	0.676	0.566
8	3.476	2.459	1.805	1.363	1.234	1.011	0.839
9	3.427	2.394	1.733	1.300	1.168	0.949	0.781
10	5.070	3.476	2.486	1.835	1.639	1.328	1.086
11	4.989	3.371	2.375	1.733	1.544	1.238	1.007
12	3.337	2.215	1.551	1.116	0.991	0.790	0.639
13	4.753	3.124	2.141	1.536	1.356	1.072	0.861
14	3.688	2.377	1.617	1.149	1.014	0.800	0.636
15	4.969	3.185	2.151	1.518	1.332	1.046	0.834
16	4.407	2.786	1.873	1.309	1.153	0.901	0.713
17	4.681	2.936	1.969	1.375	1.208	0.943	0.748
18	4.374	2.737	1.818	1.260	1.106	0.860	0.683
19	5.442	3.393	2.248	1.559	1.369	1.064	0.842
20	6.217	3.798	2.503	1.728	1.514	1.171	0.926
21	5.233	3.183	2.088	1.435	1.258	0.969	0.765
22	6.080	3.713	2.407	1.663	1.446	1.120	0.876
23	6.990	4.235	2.752	1.890	1.640	1.265	0.995
24	11.213	6.759	4.377	2.988	2.613	2.000	1.571
25	6.890	4.133	2.667	1.815	1.582	1.213	0.950
26	6.886	4.100	2.629	1.786	1.556	1.196	0.939
27	8.560	5.000	3.194	2.173	1.881	1.443	1.130
28	7.593	4.404	2.824	1.898	1.641	1.254	0.979
29	6.744	3.910	2.467	1.660	1.431	1.094	0.850
30	6.507	3.742	2.353	1.574	1.353	1.030	0.804

[1] Maximum acceleration value considered for the soil at all M_w.

Thus, using Youd and Idrisss Equation (4) [2], the SF_{liq} values presented in Table 4 were graphically represented in Figure 9 for seven different values of earthquake intensity: 3.5, 4.0, 4.5, 5.0, 5.2, 5.6, and 6.0 (it must be taken into account that the scale of the moment is logarithmic, not linear). The extreme values chosen are those that are considered limits: on the one hand, earthquakes lower than 3.5 M_w do not usually produce or induce liquefaction processes [2], while the earthquake of M_w 6.0 is close to the maximum value expected in the area, according to Torres [8] and the Ambraseys relation [38] between M_w and epicentral distance R_e (in kilometers) (see Figure 8).

$$M_w = -0.31 + 2.65\ 10^{-8}\ R_e + 0.99\ log\ (R_e) \quad (5)$$

It can be seen that when the M_w is strictly under 4.0, seismic forces cannot produce any liquefaction process, in analyzing the obtained results (see Table 4). For the M_w 4.0 value, the first 3 m of sediments could have the probability to liquefy. That depth is increasing, and also the SF_{liq} is decreasing for 4.5 (6 m), 5.0 (7 m), and 5.2 (7 m) M_w earthquake moments. At the 5.6 M_w value, the first 9.0 m of sediments have safety values under 1.0 and the first 7.0 m under 0.65. Moreover, if the 6.0 M_w is considered, all 30 m of the investigated sediments have the potential to liquefy.

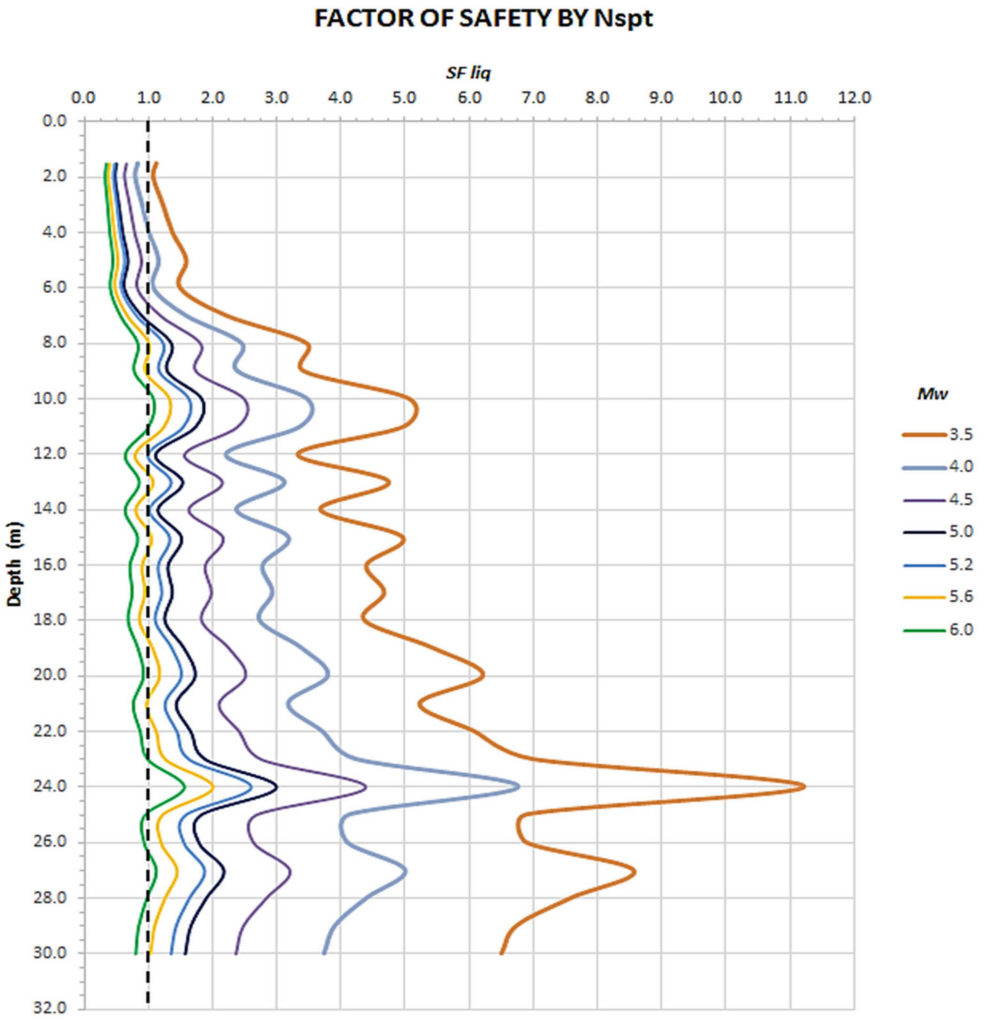

Figure 9. A graphic representation of Table 4 data where the variation of the SF_{liq} versus depth is displayed for the P-8A borehole for different moments of earthquake magnitude M_w (in color scale). A black dotted line indicates the safety factor value where liquefaction processes can occur (1.0).

From values lower than 5.6 at the moment magnitude (M_w), the affected depth with liquefaction capacity rises to 7.0 m, even for an earthquake value on the order of moment magnitude 4.5 M_w. For that, together with the saturation (a water table that could reach the surface in rainy times), the high permeability values of these materials (established at 10^{-4} m/s according to field tests up to 30.0 m depth in that area), and the low compactness of the first sedimentary levels (which is reflected in the P wave velocity values obtained, which are 430 m/s up to 10.4 m and 860 m/s up to 18.3 m depth from the surface) gives a high probability of a liquefaction phenomenon occurring in the first 7.0 m of sediment thickness [7].

5. Discussion

Measuring microtremors or ambient noise using the HVSR seismic technique is an easy, quick, and inexpensive way to define the terrain's fundamental frequency [39–41]. It is based on the existence of a two-layer geological model: sedimentary material (such as soil or recent sediments) found over a rocky basement or a compact one [11,39]. This technique has been widely validated for this purpose by various authors [39–45]. One of the strengths of that seismic survey is its repeatability and the robustness of the measurements, which provides excellent support for its use [11,39–41].

The analysis of liquefaction using this technique is also supported by authors, including a variety of research places [46–53], where they provide the application of the technique endorsed by data from recent earthquakes and their liquefaction effect in different environments. Using the K_g index or the *GSS* value, researchers considered that this technique could be applicable as a reliable tool for delimiting areas with potential susceptibility to liquefaction. Most of the studies related to this type of investigations only use the HVSR surveys results without further comparison with other analysis techniques than assume the Nakamura's vulnerability index K_g is valid [11].

A comparison between the three most used tests applied to assessing liquefaction resistance is summarized in Table 5. Seismic measures have important advantages such as their easy and quick application, repeatability (high in HVSR case [39]), and their ability to analyze all types of materials in situ (from bulk and no disturbed ways). On the other hand, the first disadvantage is the small strain analyzed, and the second is the possibility of undefined thin layers of materials (where no samples can be obtained).

Table 5. Comparison between four tests for assessing the liquefaction resistance (modified from [2]).

Feature	Test Type			
	SPT	***CPT***	***Vs***	***HVSR***
Past measurements at liquefaction sites	Abundant	Abundant	Limited	Limited
Type of stress–strain behavior influencing test	Partially drained, large strain	Drained, large strain	Small strain	Small strain
Quality control and repeatability	Poor to good	Very good	Good	Very good
Detection of the variability of soil deposits	Good for closely spaced test	Very good	Fair	Limited
Soil types in which testing is recommended	Fine under gravel	Fine under gravel	All	All
Soil sample retrieved	Yes	No	No	No
Test measures index or engineering property	Index	Index	Engineering	Index

As Andrus and Stokoe and other authors developed, using V_s as a field index is soundly based because the *CRR* and V_s are similar criteria but not in proportion. Both are related to void ratio, effective confining stresses, stress history, and geologic age [45–58].

However, in cases of difficult access, the adaptability of seismic surveys, such as HVSR to complement the preferred practice (drill boreholes or conduct in situ tests), delineating the liquefiable strata or applied them alone could be successful. Even in the presence of graveled materials, alternation or presence of gravel strata, intercalation of cemented soils, or even the phreatic level, seismic surveys can provide a good solution.

Surface processes of liquefaction are triggered by the occurrence of earthquakes whose magnitudes exceed M_w~4.0 to 4.5 (not only magnitude but frequency and duration are characteristics that are related to the triggering of those processes). This is widely known and has been studied; it could be considered that an M_w = 5.0 could be a suitable limit for defining an earthquake as a trigger. However, earth levees or dams could be more sensitive and could be affected by the abovementioned values [59].

Between the end of 2016 and the first months of 2017, the Cayambe volcano experienced anomalous seismic activity [15]. This was characterized by an increase in volcano-tectonic-type earthquakes (from internal fractures) and long-period-type earthquakes (from internal fluid and magma movements) located between 2 and 8 km below the summit. These seismic events were more intense than the 1995 past episode [15], reaching a magnitude close to but under M_w 4.0 (see Figure 10A). All this activity was related to the Chingual fault system and the volcano activity toward the northern area of the volcano building, i.e., the area where the San Marcos dam was located (see Figure 10B). This type of scenario, although the lowest in intensity (S0 to S1) considered by the IG-EPN monitorization team, was close to the S3 "San Marcos-type", which produced the natural San Marcos dam and then the lagoon [8,15]. The potential impact of this seismic activity on the surrounding area could be significant, and that research is crucial in understanding this impact.

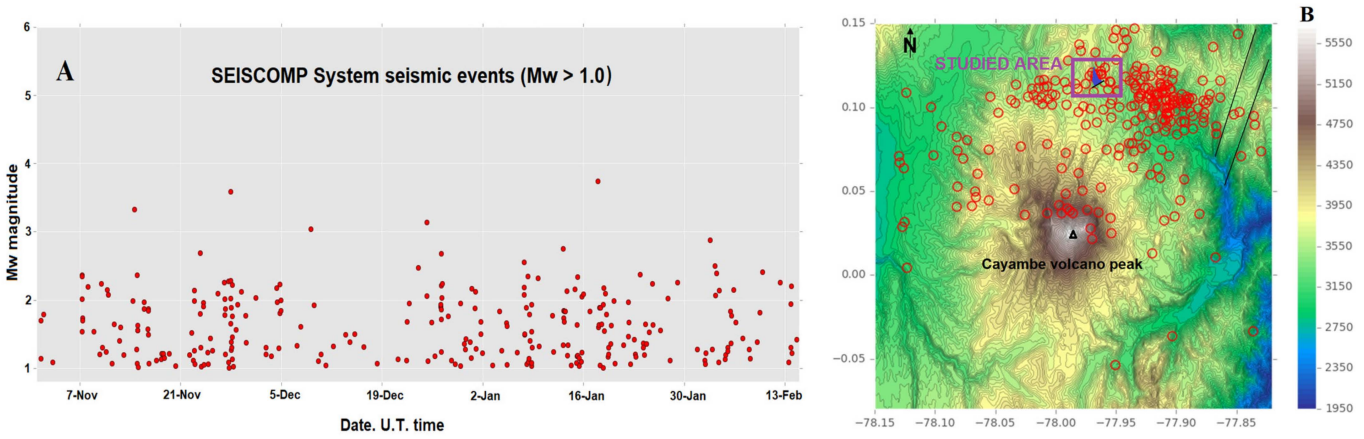

Figure 10. (**A**) The seismic events measured between 7 November 2016 and 13 February 2017 (SEISCOMP system, events with M_w > 1.0) in the ANGU Cayambe volcano seismic station (modified from [15]). (**B**) Seismic events near the Cayambe volcano peak from early June 2016 to February 2017. The black lines to the northeast of the figure correspond to the segments of the Chingual fault system, and the San Marcos dam studies area is also indicated (modified from [15]).

Thus, it must be considered that in the possibility of reaching an event of the S3 scenario, the seismic activity and its associated earthquakes could potentially reach magnitudes between M_w 4.0 and 5.0 or even exceed this range. From the previous analysis, the low limit of earthquake magnitude was established under 4.0, and 4.5 is a magnitude that can trigger liquefaction processes (see Table 4 and Figure 9). The actual volcanic activity (from the end of 2017) has returned to low levels but is still occurring.

Reviewing the literature, the larger the K_g index values, the greater the susceptibility of materials to liquefy, but from a qualitative point of view; one is the regional character of the HVSR results, both f_o and Ao, and so the K_g values result [24,41]. Some authors select different limit values for liquefaction processes starting from those that differ from 10 as the limit value indicated by Nakamura [28]: K_g > 1.7 [60], K_g > 3.5 [21], K_g > 5 [33], or K_g > 20 [30]. The established value in this research (K_g > 8) is a locally valid value for that area supported by the analyzed SPTs. Also, Singh et al. [61] indicate that this is evident when an increase in amplitudes (A_o) occurs at low fundamental frequencies (f_o), being where the K_g exceeds 20; the liquefaction processes and its effects are up to 30% from others under that value. Thus, that index could be a vulnerability delimitation parameter for determining weak areas with potential susceptibility to liquefy [29,62].

In southern Iran, Mokhberi and Yazdanpanah [60] performed an analysis of liquefaction features comparing with borehole SPTs (using M_w of 6.5 and 7.5 and for 245 Gal acceleration) over a sedimentary thin layer of sandy soil (SP-SM) deposited over weak marl-silty soil. The basement (sandstones, clay, and marly-clay intercalated rocks) is 2 to 8 m in depth, being weathered in the upper part but reaching V_s values close to rock definition (~550 m/s) [11,12]. The present study investigated thicker fluvio-glacial and volcanic sedimentary (~30 m) layers, which present the phreatic level close to the surface (under saturation conditions), making materials more prone to liquefy than dry soils. Also, considering the thickness and the PGA affectation, both are higher than those in [60], being the SF_{liq} calculated and analyzed for seven cases of different M_w moment magnitudes (including the volcano-type earthquakes). Moreover, all parameters used here were calculated for that area, and the results were more accurate than those applied from broad values.

The study analyzed the applicability of the HVSR technique in delimitating the prone-to-liquefy areas, but it can also be used considering the geology and geological processes [20,39,42]. Some authors' analyses were based on ambient noise or natural vibrations performed as a stand-alone tool. They showed K_g parameter distribution maps to evaluate the liquefaction susceptibility without having a contrast of direct sampling techniques or laboratory essays, which could be considered a general interpretation [23,42,47,49,50].

6. Conclusions

The foundation area of the San Marcos dam was tested for the liquefaction potential using the HVSR technique at 20 single station points. The natural vibration frequency f_o and its associated value of the H/V spectral ratio (A_o) were obtained with a range of values between 0.12 Hz and 61.26 Hz and from 0.95 to 9.33 for A_o (dimensionless).

Based on those HVSR parameters from data processing, the K_g (dimensionless) value was calculated for each of the points according to Nakamura's formulation [11]. Additionally, the ground shear stress value for a site acceleration of $0.331g$ and an M_w 5.0 earthquake moment was determined (from PSHA and conditions expressed in [8,16]). The results defined that the areas around the P-8A borehole, drilling in the central area of the dam, and the valley have a high susceptibility to liquefaction based on microtremor measurements (using *GSS* and K_g values).

A comprehensive analysis of the liquefaction susceptibility factor (SF_{liq}) was conducted for this area. The analysis was based on the impact of the SPTs (procedure from Youd and Idriss [2]) for local or site effect conditions, with an acceleration of $0.51g$ (501 Gal) and earthquake design moments from M_w = 3.5 to a maximum of M_w = 6.0. Under these conditions, the entire P-8A analyzed survey (30 m) column for the maximum earthquake moment showed a liquefaction safety factor value of less than one, indicating a potential risk. No liquefaction potential was observed for strictly earthquake moments less than 4.0, further validating our thorough analysis.

The SF_{liq} variation for earthquake M_w moments from 4.0 to 5.6 (expected value as maximum from volcano activity) was observed under 1.0 for the first 7.5 m of sedimentary surface materials, so the value of this factor indicates the potentiality of liquefying processes to appear. Taking into account the results, the high level of the water table position (2.0 m depth), the high permeability values of the surface materials, as well as their low compactness (from seismic P-wave velocity), it can be concluded that the central area of the San Marcos lagoon dam has characteristics of high probability of suffering liquefaction under earthquake conditions with moment magnitudes over 4.0 M_w.

Microtremor measurements through HVSR tests can be considered a powerful technique in the definition of liquefaction-susceptible areas using the pair of values obtained from the process and the calculation of the vulnerability index (f_o, A_o, and K_g index). This technique is quick, easy to apply and process, robust and repeatable, and low cost. It is a powerful tool in identifying liquefaction-susceptible areas, especially when combined with direct surveys and laboratory essays. Also, microtremor parameters are useful in different geological conditions and materials and can be applied to liquefaction analysis over almost all places due to their robustness.

However, this tool is a qualitative approximation because it does not have the ability to define a quantitative valuation layer-per-layer, depth of affected materials, or to identify thin layers; adding no definition of the earthquake moment at which the processes could start. Also, it is highly recommended that a dense mesh of measures be applied to achieve accuracy, especially in places with lateral variations in facies or materials (complex geology).

The HVSR technique has been demonstrated to be a valid and robust test for liquefaction analysis, with its respective limitations being the K_g vulnerability index, which is a proxy to define potential areas or for previous analyses of liquefaction risk. It can quickly and effectively indicate areas with probability or susceptibility to suffer this phenomenon.

Author Contributions: Conceptualization, O.A.-P. and G.T.; methodology, O.A.-P. and F.J.T.; validation, O.A.-P., F.J.T., and G.T.; formal analysis, F.J.T.; investigation, O.A.-P. and G.T.; resources, O.A.-P.; data curation, F.J.T.; writing—original draft preparation, O.A.-P. and G.T.; writing—review and editing, F.J.T.; visualization, G.T.; supervision, F.J.T. All authors have read and agreed to the published version of the manuscript.

Funding: This research received no external funding.

Data Availability Statement: The data are available upon request.

Acknowledgments: This research did not receive any specific grants from funding agencies in the public, commercial, or not-for-profit sectors. Special thanks to the Dirección del Canal de Riego Cayambe-Pedro Moncayo (GAD de la Provincia de Pichincha) and its director for letting us use the base information and access the place. Also, we want to thank Geotop Ecuatorial Consulting (geotop.equatorial@gmail.com) for the support provided and the equipment used in the research.

Conflicts of Interest: The authors declare no conflicts of interest.

References

1. Youd, T.L. Discussion of "Brief Review of Liquefaction during Earthquakes in Japan". *Soils Found.* **1977**, *17*, 82–85.
2. Youd, T.L.; Idriss, I.M. Liquefaction Resistance of Soils: Summary Report from the 1996 NCEER and 1998 NCEER/NSF Workshops on Evaluation of Liquefaction Resistance of Soils. *J. Geotech. Geoenviron. Eng.* **2001**, *127*, 817–833. [CrossRef]
3. Setiawan, H.; Serikawa, Y.; Sugita, W.; Kawasaki, H.; Miyajima, M. Experimental Study on Mitigation of Liquefaction-Induced Vertical Ground Displacement by Using Gravel and Geosynthetics. *Geoenviron. Disasters* **2018**, *5*, 22. [CrossRef]
4. Galli, P. New Empirical Relationships between Magnitude and Distance for Liquefaction. *Tectonophysics* **2000**, *324*, 169–187. [CrossRef]
5. IG-EPN Informe Sísmico Especial N. 7 2016, 2012. Available online: https://www.igepn.edu.ec/servicios/noticias/1311-informe-sismico-especial-n-7-2016 (accessed on 18 August 2023).
6. Foster, M.; Fell, R.; Spannagle, M. The Statistics of Embankment Dam Failures and Accidents. *Can. Geotech. J.* **2000**, *37*, 1000–1024. [CrossRef]
7. GADPP—Gobierno Autónomo Descentralizado de la Provincia de Pichincha. *Estudios de Geología y Geotecnia Dentro Del Proyecto de Riego Cayambe Tabacundo y Agua Potable Pesillo-Imbabura, Cantón Cayambe, Provincia de Pichincha*; GAD Provincia de Pichincha: Quito, Ecuador, 2009; p. 250.
8. Torres, G. La Amenaza Sísmica y Volcánica de la Presa de la Laguna San Marcos. Cayambe-Pichincha. Bachelor's Thesis, FIGEMPA—Universidad Central del Ecuador, Quito, Ecuador, 2018. Available online: http://www.dspace.uce.edu.ec/handle/25000/16316 (accessed on 1 August 2022).
9. Alonso-Pandavenes, O.; Torres, G.; Torrijo, F.J.; Garzón-Roca, J. Basement Tectonic Structure and Sediment Thickness of a Valley Defined Using HVSR Geophysical Investigation, Azuela Valley, Ecuador. *Bull. Eng. Geol. Environ.* **2022**, *81*, 210. [CrossRef]
10. Daag, A.; Aque, L.E.; Locaba, O.; Grutas, R.; Solidum, R. Site Response Measurements and Implications to Soil Liquefaction Potential Using Microtremor H/V in Greater Metro Manila, Philippines. *Geomat. Nat. Hazards Risk* **2023**, *14*, 2256936. [CrossRef]
11. Nakamura, Y. A Method for Dynamic Characteristics Estimation of Subsurface Using Microtremor on the Ground Surface. *Q. Rep. Railw. Tech. Res.* **1989**, *30*, 25–33.
12. Nakamura, Y. Seismic Vulnerability Indices for Ground and Structures Using Microtremor. In Proceedings of the World Congress, Florence, Italy, 17–19 September 1997; p. 7.
13. Samaniego, P.; Monzier, M.; Robin, C.; Hall, M.L. Late Holocene Eruptive Activity at Nevado Cayambe Volcano, Ecuador. *Bull. Volcanol.* **1998**, *59*, 451–459. [CrossRef]
14. Bernard, B.; Samaniego, P. Escenarios Eruptivos En El Volcán Cayambe y Construcción de Un Árbol de Eventos. In Proceedings of the III Jornadas en Ciencias de la Tierra, Quito, Ecuador, 8–12 May 2017.
15. IG-EPN Informe Anual de La Actividad Del Volcán Cayambe 2017. Available online: https://www.igepn.edu.ec/servicios/busqueda-informes (accessed on 18 August 2023).
16. MIDUVI—Ministerio de Desarrollo Urbano y Vivienda. Gobierno de la República de Ecuador NEC-SE-DS. Peligro Sísmico, Diseño Sísmo Resistente 2015. Available online: https://www.habitatyvivienda.gob.ec/documentos-normativos-nec-norma-ecuatoriana-de-la-construccion/ (accessed on 10 September 2023).
17. Jefferies, M.; Been, K. *Soil Liquefaction*, 1st ed.; CRC Press: Boca Raton, FL, USA, 2006; ISBN 978-0-203-30196-8.
18. Ishihara, K. Liquefaction and Flow Failure during Earthquakes. *Géotechnique* **1993**, *43*, 351–451. [CrossRef]
19. Ishihara, K. *Soil Behaviour in Earthquake Geotechnics*; Oxford Engineering Science Series; 1ª Oxford Science Publications; Clarendon Press: Oxford, UK, 1996; ISBN 0-19-856224-1.
20. Nakamura, Y.; Takizawa, T. Evaluation of Liquefaction of Surface Ground Using Microtremor. *Proc. 45th Annu. Meet. JSCE Tokio* **1990**, *1*, 1068–1069.
21. Uehan, F.; Nakamura, Y. *Ground Motion Characteristics Around Kobe City Detected by Microtremor Measurement*; Elsevier Science Ltd.: Acapulco, Mexico, 1996; Volume 714, p. 8.
22. Massa, M.; Mascandola, C.; Lovati, S.; Carannante, S.; Morasca, P.; D'Alema, E.; Franceschina, G.; Gomez, A.; Poggi, V.; Martelli, L.; et al. Seismic and Geological Bedrock Depth Estimation at Cavezzo Site (Po Plain, Northern Italy): Example of Passive Geophysical Survey in the Assessment of Soil Liquefaction Potential. In Proceedings of the EGU General Assembly Conference Abstracts, Vienna, Austria, 8–13 April 2018; p. 7882.
23. Kusuma, W.H.; Sanny, T.A. Analysis of Ground Shear Strain (GSS) In Mapping, Liquefaction Vulnerability Potential Using HVSR (Horizontal to Vertical Spectral Ratio) Method. Case Study: Sepaku Subdistrict, North Penajam Paser Regency, East Kalimantan. *IOP Conf. Ser. Earth Environ. Sci.* **2022**, *1031*, 012027. [CrossRef]

24. Putra, R.R.; Kiyono, J.; Agung, D. Liquefaction Potential Based on Ground Investigation Data and Natural Frequency. *Bull. Earthq. Eng.* **2022**, *20*, 15.
25. Moreno Robles, J. El Fenómeno de La Licuación Por Flujo. Aproximación Teórica y Práctica. *Geotecnia* **2022**, *156*, 3–32. [CrossRef]
26. Seed, H.B.; Idriss, I.M. Simplified Procedure for Evaluating Soil Liquefaction Potential. *J. Soil Mech. Found. Div.* **1971**, *97*, 1249–1273. [CrossRef]
27. Seed, H.B.; Tokimatsu, K.; Harder, L.F.; Chung, R.M. Influence of SPT Procedures in Soil Liquefaction Resistance Evaluations. *J. Geotech. Engrg.* **1985**, *111*, 1425–1445. [CrossRef]
28. Nakamura, Y. Clear Identification of Fundamental Idea of Nakamura's Technique and Its Applications. In Proceedings of the 12th World Conference on Earthquake Engineering, Auckland, New Zealand, 30 January–4 February 2000.
29. Huang, H.-C.; Tseng, Y.-S. Characteristics of Soil Liquefaction Using H/V of Microtremors in Yuan-Lin Area, Taiwan. *Terr. Atmos. Ocean. Sci.* **2002**, *13*, 325. [CrossRef]
30. Fergany, E.; Omar, K. Liquefaction Potential of Nile Delta, Egypt. *NRIAG J. Astron. Geophys.* **2017**, *6*, 60–67. [CrossRef]
31. Yulianur, A.; Saidi, T.; Setiawan, B.; Sugianto, S.; Rusdi, M. Microtremor Measurement at Liquefaction-Induced Ground Deformation Area. *J. Eng. Sci. Technol.* **2020**, *15*, 19.
32. Kang, S.Y.; Kim, K.-H.; Gihm, Y.S.; Kim, B. Soil Liquefaction Potential Assessment Using Ambient Noise: A Case Study in Pohang, Korea. *Front. Earth Sci.* **2022**, *10*, 1029996. [CrossRef]
33. Abdelrahman, K.; Al-Amri, A.M.; Alzahrani, H.; Qaysi, S.; Al-Otaibi, N. Soil Liquefaction Susceptibility of Jizan Coastal Area, Southwest Saudi Arabia, Based on Microtremor Measurements. *Arab. J. Geosci.* **2022**, *15*, 611. [CrossRef]
34. Uyanık, O. Soil Liquefaction Analysis Based on Soil and Earthquake Parameters. *J. Appl. Geophys.* **2020**, *176*, 104004. [CrossRef]
35. SESAME Project. *Guidelines for the Implementation of the H/V Spectral Ratio Technique on Ambient Vibrations Measurements, Processing and Interpretation*; European Commission: Grenoble, France, 2004; p. 62.
36. Wathelet, M.; Chatelain, J.-L.; Cornou, C.; Giulio, G.D.; Guillier, B.; Ohrnberger, M.; Savvaidis, A. Geopsy: A User-Friendly Open-Source Tool Set for Ambient Vibration Processing. *Seismol. Res. Lett.* **2020**, *91*, 1878–1889. [CrossRef]
37. Sil, A.; Haloi, J. Empirical Correlations with Standard Penetration Test (SPT)-N for Estimating Shear Wave Velocity Applicable to Any Region. *Int. J. Geosynth. Ground Eng.* **2017**, *3*, 22. [CrossRef]
38. Ambraseys, N.N. Engineering Seismology: Part II. *Earthq. Engng. Struct. Dyn.* **1988**, *17*, 51–105. [CrossRef]
39. Alonso Pandavenes, O. Técnicas de Sísmica Pasiva HVSR Aplicadas a la Geotecnia. Aplicación al Estudio de Movimientos en Masa en la Planificación Territorial e Infraestructura Civil en Ecuador. Ph.D. Thesis, Universitat Politècnica de València, Escuela Técnica Superior de Ingenieros de Caminos, Canales y Puertos, Valencia, Spain, 2024.
40. Alonso-Pandavenes, O.; Torrijo, F.J.; Garzón-Roca, J.; Gracia, A. Early Investigation of a Landslide Sliding Surface by HVSR and VES Geophysical Techniques Combined, a Case Study in Guarumales (Ecuador). *Appl. Sci.* **2023**, *13*, 1023. [CrossRef]
41. Alonso-Pandavenes, O.; Bernal, D.; Torrijo, F.J.; Garzón-Roca, J. A Comparative Analysis for Defining the Sliding Surface and Internal Structure in an Active Landslide Using the HVSR Passive Geophysical Technique in Pujilí (Cotopaxi), Ecuador. *Land* **2023**, *12*, 961. [CrossRef]
42. Molnar, S.; Cassidy, J.F.; Castellaro, S.; Cornou, C.; Crow, H.; Hunter, J.A.; Matsushima, S.; Sánchez-Sesma, F.J.; Yong, A. Application of Microtremor Horizontal-to-Vertical Spectral Ratio (MHVSR) Analysis for Site Characterization: State of the Art. *Surv. Geophys.* **2018**, *39*, 613–631. [CrossRef]
43. Sebastiano, D.; Francesco, P.; Salvatore, M.; Roberto, I.; Antonella, P.; Giuseppe, L.; Pauline, G.; Daniela, F. Ambient Noise Techniques to Study Near-Surface in Particular Geological Conditions: A Brief Review. In *Innovation in Near-Surface Geophysics*; Elsevier: Amsterdam, The Netherlands, 2019; pp. 419–460. ISBN 978-0-12-812429-1.
44. Lermo, J.; Chávez-García, F.J. Site Effect Evaluation Using Spectral Ratios with Only One Station. *Bull. Seismol. Soc. Am.* **1993**, *83*, 1574–1594. [CrossRef]
45. Delgado, J.; López Casado, C.; Giner, J.; Estévez, A.; Cuenca, A.; Molina, S. Microtremors as a Geophysical Exploration Tool: Applications and Limitations. *Pure Appl. Geophys.* **2000**, *157*, 1445–1462. [CrossRef]
46. Yuliyanto, G.; Harmoko, U.; Widada, S. Identification of Potential Ground Motion Using the HVSR Ground Shear Strain Approach in Wirogomo Area, Banyubiru Subdistrict, Semarang Regency. *Int. J. Appl. Environ. Sci.* **2016**, *11*, 1497–1507.
47. Aque, L.E.G.; Daag, A.S.; Grutas, R.N.; Abigania, M.I.T.; Dizon, M.P.; Buhay, D.J.L.; Mitiam, E.D.; Serrano, A.T.; Halasan, O.P.C.; Reyes, M.J.V.; et al. Evaluation of Passive Seismic Horizontal-To-Vertical Spectral Ratio (HVSR) for rapid Site-Specific Liquefaction Hazard Assessment. In Proceedings of the 18th Annual Meeting of the Asia Oceania Geosciences Society, Singapore, 1–6 August 2021; World Scientific: Singapore, 2022; pp. 132–134.
48. Herrera, M.; Arango, S.; Cruz, A.; Sandoval, E.; Thomson, P. Assessment of Nakamura Methodology for Evaluating Soil Liquefaction Potential. In Proceedings of the Geotechnical Earthquake Engineering and Soil Dynamics V, Austin, TX, USA, 10–13 June 2018; American Society of Civil Engineers: Austin, TX, USA, 2018; pp. 94–107.
49. Khan, M.Y.; Turab, S.A.; Ali, L.; Shah, M.T.; Qadri, S.M.T.; Latif, K.; Kanli, A.I.; Akhter, M.G. The Dynamic Response of Coseismic Liquefaction-Induced Ruptures Associated with the 2019 M_w 5.8 Mirpur, Pakistan, Earthquake Using HVSR Measurements. *Lead. Edge* **2021**, *40*, 590–600. [CrossRef]
50. Meng, Q.; Li, Y.; Wang, W.; Chen, Y.; Wang, S. A Case Study Assessing the Liquefaction Hazards of Silt Sediments Based on the Horizontal-to-Vertical Spectral Ratio Method. *J. Mar. Sci. Eng.* **2023**, *11*, 104. [CrossRef]

51. Ramos, A.; Viana da Fonseca, A.; Carrilho Gomes, R. Evaluating Soil Liquefaction Potential Using Nakamura Methodology in an Experimental Site. In *Earthquake Geotechnical Engineering for Protection and Development of Environment and Constructions, Proceedings of the 7th International Conference on Earthquake Geotechnical Engineering, (ICEGE 2019), Rome, Italy, 17–20 June 2019*; CRC Press: Rome, Italy, 2019; p. 5998. ISBN 978-0-429-03127-4.
52. Andrus, R.D.; Stokoe II, K.H. Liquefaction Resistance of Soils from Shear-Wave Velocity. *J. Geotech. Geoenviron. Eng.* **2000**, *126*, 1015–1025. [CrossRef]
53. Iwasaki, T.; Tokida, K.; Tatsuoka, F.; Watanabe, S.; Yasuda, S.; Sato, H. Microzonation for Soil Liquefaction Potential Using Simplified Methods. In Proceedings of the 3rd International Conference on Microzonation, Seattle, WA, USA, 28 June–1 July 1982; Volume 3, pp. 1310–1330.
54. Huang, Y.; Yu, M. *Hazard Analysis of Seismic Soil Liquefaction*; Springer Natural Hazards; Springer Singapore: Singapore, 2017; ISBN 978-981-10-4378-9.
55. Issaadi, A.; Saadi, A.; Semmane, F.; Yelles-Chaouche, A.; Galiana-Merino, J.J. Liquefaction Potential and Vs30 Structure in the Middle-Chelif Basin, Northwestern Algeria, by Ambient Vibration Data Inversion. *Appl. Sci.* **2022**, *12*, 8069. [CrossRef]
56. Zhang, L. A Simple Method for Evaluating Liquefaction Potential from Shear Wave Velocity. *Front. Archit. Civ. Eng. China* **2010**, *4*, 178–195. [CrossRef]
57. Cetin, K.O.; Seed, R.B.; Kayen, R.E.; Moss, R.E.S.; Bilge, H.T.; Ilgac, M.; Chowdhury, K. Examination of Differences between Three SPT-Based Seismic Soil Liquefaction Triggering Relationships. *Soil Dyn. Earthq. Eng.* **2018**, *113*, 75–86. [CrossRef]
58. Andrus, R.D.; Stokoe, K.H.; Hsein Juang, C. Guide for Shear-Wave-Based Liquefaction Potential Evaluation. *Earthq. Spectra* **2004**, *20*, 285–308. [CrossRef]
59. Green, R.A.; Bommer, J.J. What Is the Smallest Earthquake Magnitude That Needs to Be Considered in Assessing Liquefaction Hazard? *Earthq. Spectra* **2019**, *35*, 1441–1464. [CrossRef]
60. Mokhberi, M.; Yazdanpanah Fard, S. Liquefaction Hazard assessment using Horizontal-to-Vertical Spectral Ratio of Microtremor. *J. Struct. Eng. Geotech.* **2018**, *8*, 31–44.
61. Singh, A.P.; Shukla, A.; Kumar, M.R.; Thakkar, M.G. Characterizing Surface Geology, Liquefaction Potential, and Maximum Intensity in the Kachchh Seismic Zone, Western India, through Microtremor Analysis. *Bull. Seismol. Soc. Am.* **2017**, *107*, 1277–1292. [CrossRef]
62. Beroya, M.A.A.; Aydin, A.; Tiglao, R.; Lasala, M. Use of Microtremor in Liquefaction Hazard Mapping. *Eng. Geol.* **2009**, *107*, 140–153. [CrossRef]